ACS APPLIED MATERIALS & INTERFACES

Research Article

www.acsami.org

Inkjet Printed Fractal-Connected Electrodes with Silver Nanoparticle Ink

Mohammad Vaseem, Kil Mok Lee, A-Ra Hong, and Yoon-Bong Hahn*

Department of BIN Fusion Technology, School of Semiconductor and Chemical Engineering, and Nanomaterials Processing Research Center, Chonbuk National University, 567 Baekje-daero, Deokjin-gu, Jeonju 561-756, Republic of Korea

Supporting Information

ABSTRACT: The development of a simple and reliable method for nanoparticles-based ink in an aqueous solution is still a challenge for its inkjet printing application. Herein, we demonstrate the inkjet printing of fractal-aggregated silver (Ag) electrode lines on substrates. Spherical, monodisperse Ag nanoparticles have been synthesized using silver nitrate as a precursor, ethylene glycol as a reducing agent, and polyvinyl pyrrollidone as a capping agent. As-synthesized pure Ag nanoparticles were well dispersed in water-ethylene glycol mixture, which was directly used as an ink for inkjet printing. Using this ink, the Ag electrodes of fractal-connected lines were printed on Si/SiO_2, glass, and polymer substrates. The fractal-connected Ag lines were attributed to the diffusion-limited aggregation of Ag nanoparticles and the effect of annealing on conductivity was also examined.

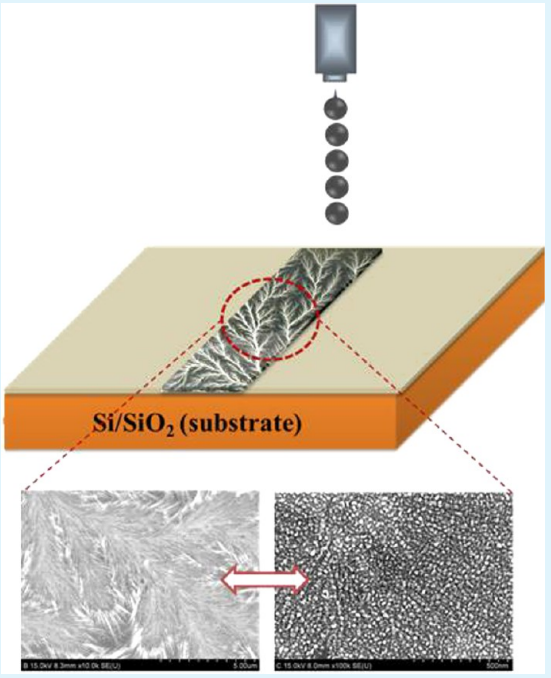

KEYWORDS: *silver NPs, inkjet printing, diffusion-limited aggregation, conductivity*

1. INTRODUCTION

Inkjet printing is an efficient alternative to conventional photolithography for producing various electronic devices and has advantages such as low cost, high-speed patterning, and applicability to various substrates.[1−15] However, most inkjet-printing applications require sophisticated synthetic procedures for preparing monodisperse nanoparticles (NPs) without particle−particle aggregation in the dispersion medium. Moreover, the NP-based ink formulation is usually restricted to NP dispersed in volatile solvents such as isopropyl alcohol (IPA), ethanol, and terpineol or in typical organic solvents such as dodecane, tolune, and butylbenzene.[16−23] It was observed that volatile nature of the solvents generally leads to a unwanted coffee-ring effect, which can degrade the quality of printed features. Therefore, the development of a simple and reliable method for nanoparticle-based ink in an aqueous solution is still a challenge for inkjet printing application. For the formulation of water-based ink, metal salt-based ink-formulation can be a choice. But recently, metal−organic silver salt for the formulation of an aqueous ink was reported for printing Ag conductive lines on the glass and PET substrates. It was observed that as compared to NPs-based ink, the salt-based ink composed of various organic residues which should be removed at an elevated temperature for better electrical behavior.[24] For materials point of view, Wang et al. developed a general strategy for the synthesis of Ag NPs that required a higher reaction temperature (≥80 °C) and longer reaction time (10 h).[25] Chen et al.[26] reported a novel two-phase procedure for the preparation of monodisperse silver NPs, but it was only suitable for the preparation of NPs stabilized by alkylamine. We observed that the amphiphlic nonionic polymer, polyvinyl pyrrolidone (PVP) has widely been used as surfactant to prevent particles from agglomerating during synthesis of various nanomaterials.[27,28] Inspired by this information, we have investivated Ag NPs in the presence of PVP as a dispersant suited for inkjet printing.

Received: April 19, 2012
Accepted: June 6, 2012
Published: June 6, 2012

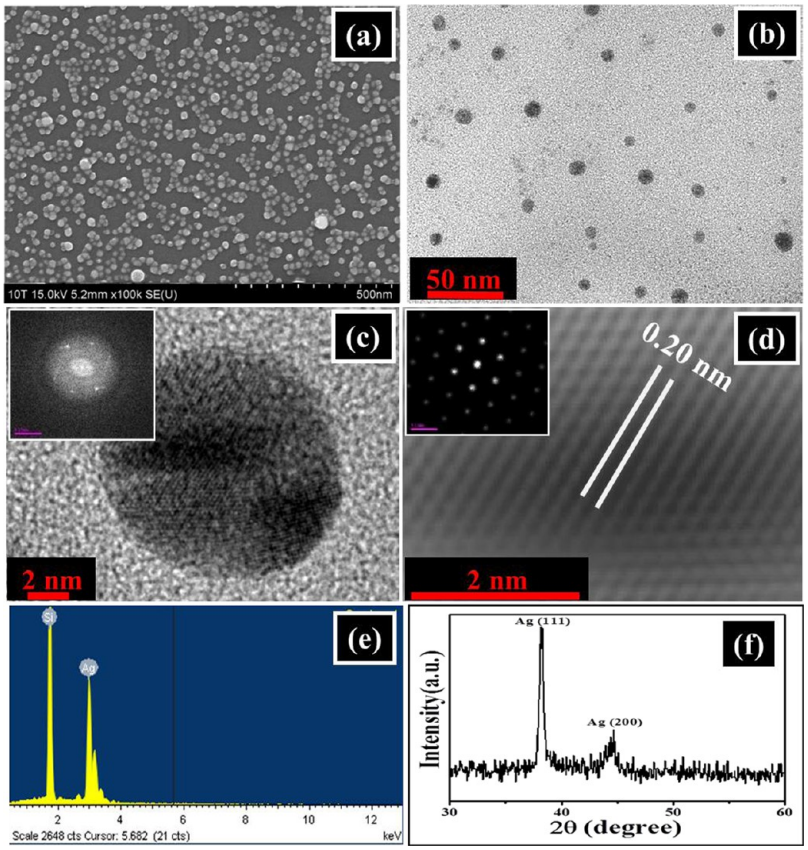

Figure 1. Typical images of (a) FESEM, (b) TEM, (c) HR-TEM, and (d) IFFT; (e) EDS spectrum and (f) XRD pattern of the Ag NPs synthesized by polyol method at 80 °C. The insets in c and d show FFT spectra and diffraction pattern, respectively.

In this paper, we reported the facile preparation of PVP-stabilized silver NPs at 80 °C for 30 min without any complex instrumental setup. As-synthesized pure Ag NPs were well dispersed in water-ethylene glycol solvent mixture which was directly used as an ink. Using the as-formulated Ag NPs ink we have successfully demonstrated jetting and writing of various overprinted Ag line patterns on substrates. Interestingly, we have observed that after printing the Ag lines on the substrate, fractal-aggregated connections were formed by the diffusion-limited aggregation (DLA) of Ag NPs. To confirm the PVP-capping over the surface of as-formulated Ag NPs ink, we also investigated an elemental mapping of single fractal aggregated morphology. As-printed Ag lines were further analyzed in terms of its resistivity with varying annealing temperature from room temperature to 300 °C.

2. EXPERIMENTAL DETAILS

Chemicals. Silver(I) nitrate ($AgNO_3$) (purity 99.9%, Samchun Pure Chemical Co., Ltd., Korea), polyvinyl pyrollidone (PVP, Sigma-Aldrich), ethylene glycol (EG) (≥99%, Sigma-Aldrich) and liq. Ammonia (28−30%, Samchun Pure Chemical Co., Ltd., Korea) were used as received without further purification.

Synthesis of Ag NPs and Ink Formulation. The synthesis process of Ag NPs involves heating a polyol (i.e., EG) with a salt precursor (silver nitrate) and a polymeric capping agent (PVP) to generate metal colloids. Silver NPs were synthesized in a refluxing pot via solution process. In a typical synthesis process, 0.5 g PVP was dissolved in 50 mL EG solution and transferred to the refluxing pot and heated until 80 °C with continuous stirring. When the resultant solution reached at 80 °C, 50 mL of 0.1 M $AgNO_3$ was added into the heated solvent by dropwise addition of ammonia until solution pH 10. After this step, the resulted mixture was kept for 30 min to complete the reduction process. The reduction reaction for the formation of silver NPs is written as

$$2CH_2OH\text{-}CH_2OH \rightarrow 2CH_3CHO + 2H_2O \quad (1)$$

$$2CH_3CHO + 2AgOH \rightarrow 2Ag + CH_3COCOCH_3 + 2H_2O \quad (2)$$

To check the effect of reaction temperature on the shape and size of as-synthesized Ag NPs, we have carried out different sets of experiments with varying reaction temperatures from 70 to 100 °C. In all the prepared samples, precursor concentration and reaction time were kept constant at 0.1 M and 30 min, respectively. For Ag NP characterization, brown-yellowish color colloidal solution of silver were centrifuged at 4000 rpm for 5 min and then washed with deionized water. For the formulation of water-based Ag ink, the weight percentage of Ag NPs:water:EG was 10:55:35. The formulated Ag ink was then filtered by 0.2 μm polypropylene (PP) whatman paper before jetting. The viscosity of as-formulated ink was 5.47 cP, measured at the spindle speed of 200 rpm and shear rate of 264 s^{-1} at room temperature. The surface tension of as-prepared ink sample was measured as 40.799 mN/m. The Ag pattern lines were directly printed on Si/SiO_2 substrates using drop-on-demand piezoelectric inkjet nozzle (manufactured by Dimatix) with diameter of 16 μm and drop volume was 10 pL. Uniform and continuous ejection of droplets was achieved by adjusting various wave-forms while applying the firing voltage of 40 V at a 40 kHz printer velocity. The jetting velocity of ejected droplets was ∼3.3 m/s. The cartridge print height was ∼0.3 mm.

Characterization. The structural investigation was carried out by field emission scanning electron microscopy (FESEM, Hitachi S4700) equipped with energy-dispersive X-ray (EDS) spectroscopy, transmission electron microscopy (TEM) equipped with digital charge-coupled device (JEOL-JEM-2010 equipped with CCD camera). For the TEM analysis the as-synthesized Ag nanoparticles diluted with

ethanol was dropped on copper grid with a perforated carbon film and dried in vacuum. The crystal phase and crystallinity were analyzed by X-ray diffractometer (XRD, Rigaku) with Cu−Kα radiation (λ = 1.54178 Å) in the range of 30−60° at 40 kV. The UV−vis absorption analysis was done by UV−vis spectrophotometer. Thermogravimetric analysis (TGA) of PVP-capped Ag NPs were performed by TGA Q50 thermal analyzer at the temperature range of 23−600 °C with a heating rate of 20 °C/min. The quality and composition of PVP-capped Ag nanoparticles sample was further characterized by the Fourier transform infrared (FTIR) spectroscopy in the wavelength range of 4000−400 cm^{-1}.

3. RESULTS AND DISCUSSION

3.1. Synthesis and Characterization of Silver NPs.

Figure 1a−f shows the structural characterization of Ag NPs synthesized by polyol method at 80 °C. The as-synthesized spherical and monodisperse Ag NPs show uniformly grown in high density with average particle size in the range of 12 ± 2 nm (a). The as-observed particle size is further confirmed by its corresponding TEM image (b, c). The products are further characterized by the inverse fast Fourier transform (IFFT) image of a single Ag NP and its corresponding diffraction pattern (d). The as-synthesized silver NPs are highly crystalline and have interplanar spacing of 0.2 nm corresponding to (100) planes of fcc silver crystal.[29,30] The perfect lattice with 6-fold symmetry rather than 4-fold symmetry is attributed to the double diffraction effects caused by the electron beam consecutively passed through the superimposed twin segments, which was also observed by Hofmeister et al.[31] The double diffraction effect can lead to anomalous images containing atomic column-like contrasts that exhibit nearly 6-fold symmetry as clearly reflected by the corresponding diffractograms (see insets in c and d). No impurities are observed in the EDS spectrum (e) and all the diffraction peaks in XRD pattern (f) are indexed to face-centered cubic silver (JCPDS NO. 04−0783)[32,33] and the strong and sharp peaks indicate that silver NPs are highly crystalline.

To examine the effect of reaction temperature on the morphological properties of as-synthesized Ag NPs, temperature-dependent experiments were performed. The obtained results in terms of FESEM and TEM images and particle size distribution showed that the particle size of Ag increases with reaction temperature (see the Supporting Information, Figure 1S). The temperature-dependent size variation of Ag NPs was further observed in UV−vis spectra (Figure 2). As the nanoparticle size increases surface plasmon peak is red-shifted (marked by arrow).[34] Interestingly, at 70 °C the UV−vis spectrum clearly showed two populations of Ag NPs in the resulted products by two clear peaks at ∼400 nm and ∼520 nm. However, silver NPs synthesized at 80−100 °C shows strong UV−vis absorption peaks at 403−420 nm, which is attributed to the surface plasmon resonance of silver NPs and confirms the high degree of their monodispersity.[35−37] It was also observed that as-synthesized Ag NPs were well dispersed due to amphiphlic nature of PVP adsorbed on surface of NPs. To confirm the effect of PVP adsorbed on the surface of Ag NPs, we performed thermal gravimetric analysis. The TGA/DTA spectra showed a weight loss of ∼4% commenced at around 150 °C, which is due to the decomposition of adsorbed PVP (Figure 3a). The FT-IR spectra of pure PVP and PVP-capped

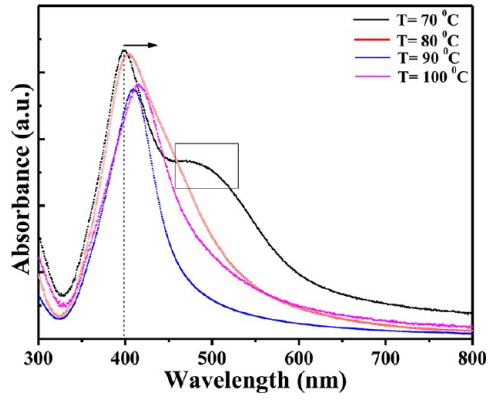

Figure 2. UV−vis spectra of Ag NPs synthesized by polyol method at different reaction temperature.

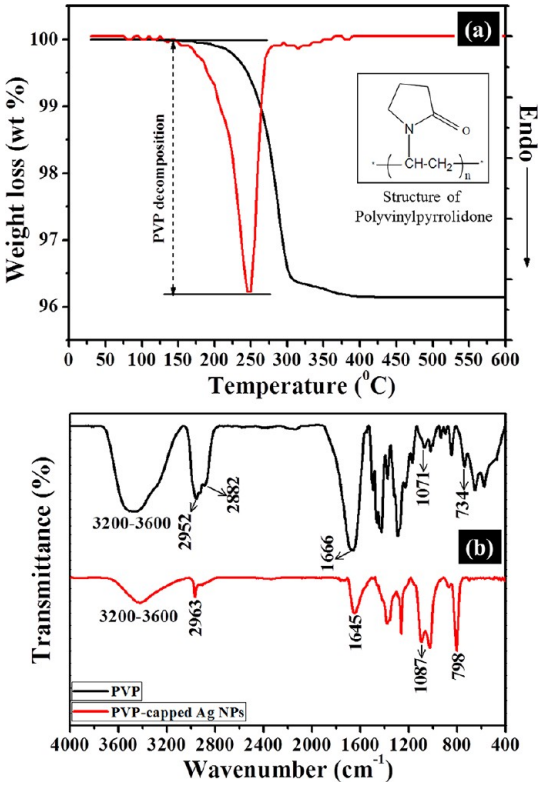

Figure 3. (a) TGA/DTA spectra and (b) FT-IR spectra for PVP-capped Ag NPs synthesized by polyol method at 80 °C.

silver NPs samples are shown in Figure 3b. For the pure PVP sample, the characteristics band at 734 cm^{-1} is due to plane bending vibration of long chain $-(CH-CH_2)_n-$. The band at 1071 cm^{-1} is due to C−N symmetric stretching vibrations, whereas the band at 1666 cm^{-1} corresponds to stretching vibration of −C═O. Three bands between 1400 and 1500 cm^{-1} are due to absorption peaks of −N−C−. The bands at 2882 and 2952 cm^{-1} are attributed to the symmetric and asymmetric stretching vibrations of $-CH_2-$, respectively. The broad absorption bands between 3200 and 3600 cm^{-1} is attributed due to the stretching vibration of adsorbed water. In the case of PVP-capped silver NPs, all the characteristics bands match to PVP. But, symmetric stretching vibration for C−N shifts from 1071 to 1087 cm^{-1} and −C═O stretching vibration also shifts from 1666 to 1645 cm^{-1}. As-shifted peak bands clearly indicate that either N or O atoms of PVP molecules interact with silver nanoparticles by chemical absorption.[38]

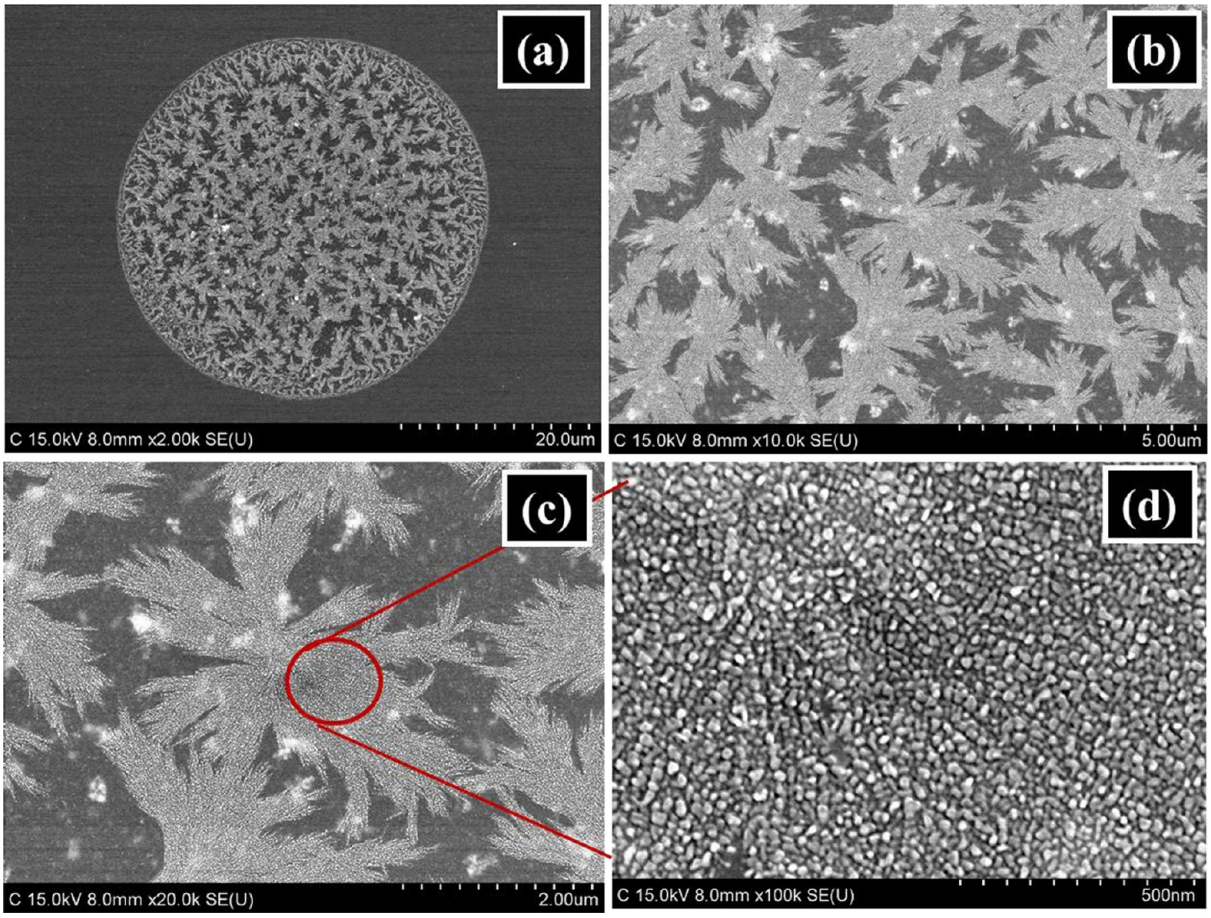

Figure 4. (a) FESEM image of single dot, (b) high-magnification FESEM image of dot area, and (c,d) FESEM images showing Ag NP-based single fractal aggregated morphology printed on Si/SiO_2 substrate with drop-spacing of 30 μm.

3.2. Ag NP Ink Formulation and Its Inkjet Printing Behavior. As-synthesized Ag NPs (the best result obtained at 80 °C) were further formulated as a water-based ink. The size distribution of Ag NPs in ink sample was monitored by dynamic light scattering (DLS) technique after filtration with 200 nm PP whatman paper (see the Supporting Information, Figure 2S). The average NPs size in the nanoink was ~12 nm. The jetting behavior of as-formulated ink was examined by printing on Si/SiO_2 substrates. Figure 4 a-d hows FESEM images of single dot formed by vertically dropped Ag ink from the nozzle, which formed dots lines on the substrate. Interestingly, we have observed that as-printed dots show fractal aggregation of Ag NPs (a). All the area of single dot covers fully with as-aggregated fractal morphology without showing any coffee-ring effect (b). When we examined single fractal morphology with high-magnification FESEM images (c, d), all the aggregated small size Ag NPs were clearly seen. It is interesting to observe that the Ag NPs prepared in water/EG shows no aggregation of nanoparticles. When these Ag NPs were printed on the Si/SiO_2 substrate from the solution, they diffused and stuck to the surface of aggregate randomly, and formed typically fractal patterns. Following the standard theory of colloids, the stability of colloid is governed by the balance between van der Waals attraction and Coulombic repulsion of charged particles.[39] Enhancing the van der Waals attraction force or weakening the Coulombic repulsion force induces a rapid coagulation of colloids. The as-formulated ink has different evaporation rates between the solvents, i.e. water (boiling temperature, T_b = 100 °C) and EG (T_b = 197 °C). When the PVP-capped Ag colloids in the form of ink were printed onto the Si/SiO_2 substrate, the evaporation of solvent resulted in the break of the force balance and thus the aggregation took place. It also can not be ruled out that capped PVP provides stearic repulsion effects in ink solution that disappear during evaporation. Such a fractal aggregation formation can also be explained by the theory proposed by Witten and Sander in 1981,[40] i.e., diffusion limited aggregation (DLA). DLA is a process whereby particles undergoing a diffusion due to the Brownian motion form aggregates of such particles and is applicable to aggregation in any system where diffusion is the primary means of transport in the system. Moreover, it is possible that because of the high evaporation rate of ethylene glycol, it may hold fractal aggregated morphology at room-temperature via diffusion limited aggregation (DLA). As-formulated Ag ink was further used to print lines on Si/SiO_2 substrates with drop-spacing of 30 μm.

Figure 5 shows FESEM images of inkjet-printed Ag lines as a function of number of overprinting. All the printed lines clearly shows fractal-aggregated connection morphology with increasing the density of Ag NPs as the number of printing increased from 1 to 5 overprinting. As it is confirmed by TGA/DTA and FT-IR analyses (see Figure 3), the silver NPs were capped with PVP molecules. To confirm this more precisely, we investigated single fractal morphology in terms of its elemental mapping. Figure 6 shows the SEM image (a) and elementals mappings (b–f) of the fractal, revealing that all the fractal morphologies

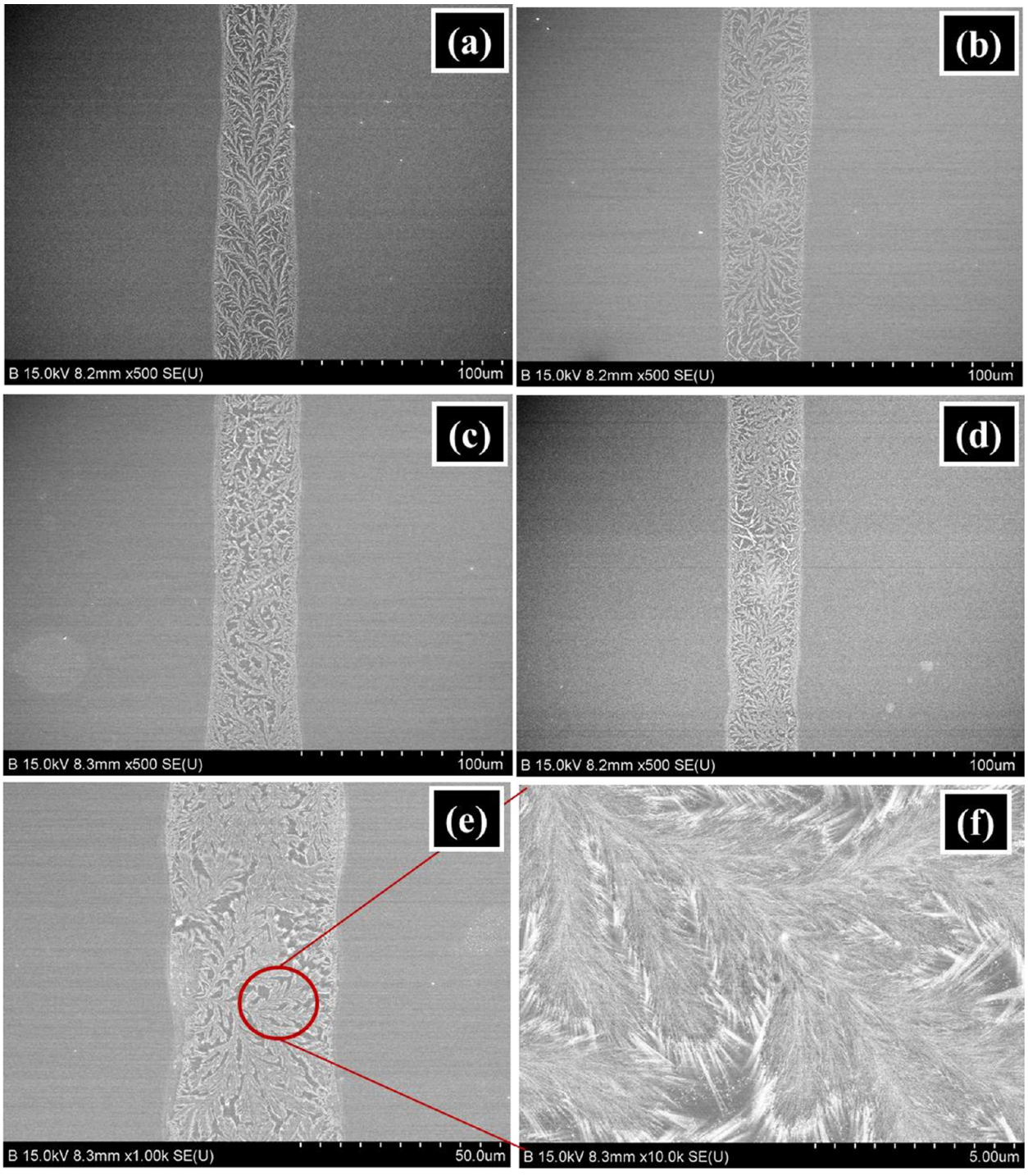

Figure 5. FESEM images of (a) 1 layer printing, (b) 2 overprinting, (c) 3 overprinting, (d) 4 overprinting, and (e, f) 5 overprinting that exhibit Ag NP-based fractal aggregated morphology printed on Si/SiO_2 substrate with drop-spacing 30 μm.

consist of silver NPs as the Ag element is detected as pink color shading (b). Moreover, excluding Ag detection other elements such as nitrogen (c), carbon (d), silicon (e), and oxygen (f) were also detected at the same area of fractal morphology, confirming PVP-capping over the surface of Ag NPs.

To check the applicability of as-formulated Ag ink on various substrates, we measured contact angle by dropping the Ag ink on four different substrates, i.e. Si/SiO_2, glass, polyethyletetraphathalate (PET), and polyimide (PI) substrates. Figure 7 shows the contact angle measurements of single droplets on the substrates. It is confirmed that as-formulated water/EG-based Ag inks show more wettability on Si/SiO_2 and glass substrates than on PET and PI substrates. Thus, as-printed dots and lines on Si/SiO_2 and glass exhibited uniform printing without showing any bulging or coffee-ring effect, but nonuniform lines patterns on PET and PI substrates due to the high contact angle were observed (see the Supporting Information, Figure 3S).

3.3. Effect of Annealing on the Printed-Pattern Morphology. To check the inkjet-printed line pattern morphology as a function of annealing temperature, 3-over printed Ag lines were annealed at 100−300 °C. Figure 8 shows

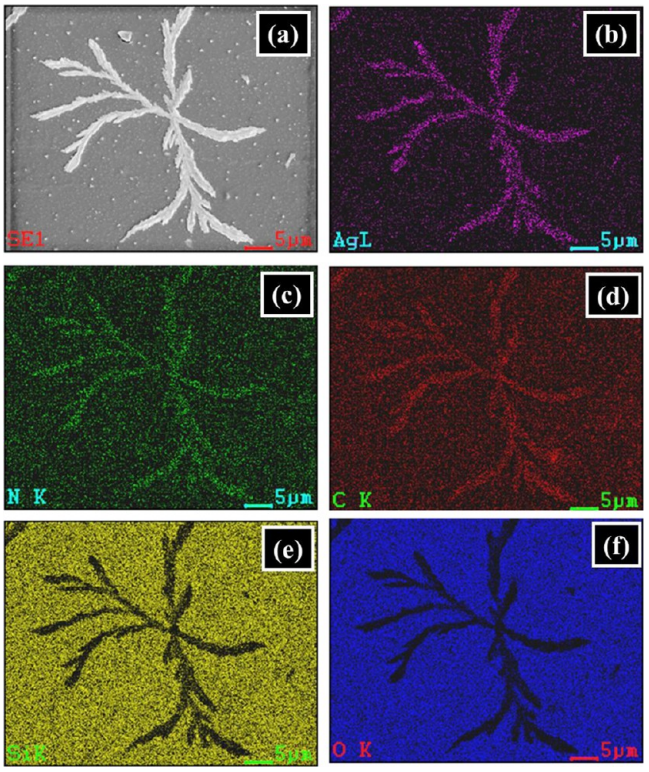

Figure 6. Elemental mapping of Ag NP-based fractal aggregated morphology: (a) SEM image, (b) Ag, (c) N, (d) C, (e) Si, and (f) O.

the microstructural evolution of the lines during the heat treatment at 25 °C (a), 100 °C (b), 150 °C (c) and 200 °C (d) for 30 min, and the resistivity variation of the Ag lines (e). The resistance (R) was measured by using a 2-point method. Generally, to ensure a conductive film the Ag nanoparticles should have a three-dimensionally interconnected conduction pathway via interparticle neck growth.[18] In this regard, it is believed from the SEM images and resistivity variation that the interparticle necking starts at 100 °C, but the DLA begins to diminish. The films annealed at above 100 °C show a dramatic change in the particle shape from discrete-and-spherical particles to continuous-and-sintered particles. In addition, heat-treatment at higher temperatures densifies the films associated with grain growth. Further densification at temperatures higher than 200 °C does not increase much in the conductivity, which is consistent with the percolation theory.[41] The electrical resistivity (ρ) of an inkjet-printed line was then calculated using $\rho = RA/l$, where R, l, and A are the resistance, the length, and the cross-sectional area of the line, respectively. The conductivity was substantially improved with heat treatment and saturated at above 200 °C, showing the resistivity of $\sim 1 \times 10^{-5}$ Ωcm.

4. CONCLUSIONS

In conclusion, nanocrystalline Ag NPs (12 ± 2 nm) have been synthesized via polyol method in presence of PVP as a dispersing agent and ethylene glycol as a reducing agent. Temperature-dependent reaction was performed which confirmed that reaction temperature affected the morphology and size of Ag NPs. The Ag NPs synthesized at 80 °C for 30 min showed almost uniform shape and size, and were well dispersed in water-ethylene glycol mixture which was directly used as an ink for inkjet printing. The as-synthesized Ag NPs at 80 °C were further formulated as a water-based ink to be used for inkjet printing application. Using the as-formulated Ag NPs inks, we have successfully printed Ag-conducting lines on the Si/SiO_2 substrates. Interestingly, we have observed that Ag-NPs printed on Si/SiO_2 substrates resulted in the formation of fractal-aggregated connection of silver lines, which was formed probably due to the diffusion-limited aggregation (DLA). Moreover, the resistivity of as-printed Ag line was observed as a function of annealing temperature and showed $\sim 1 \times 10^{-5}$ Ω cm.

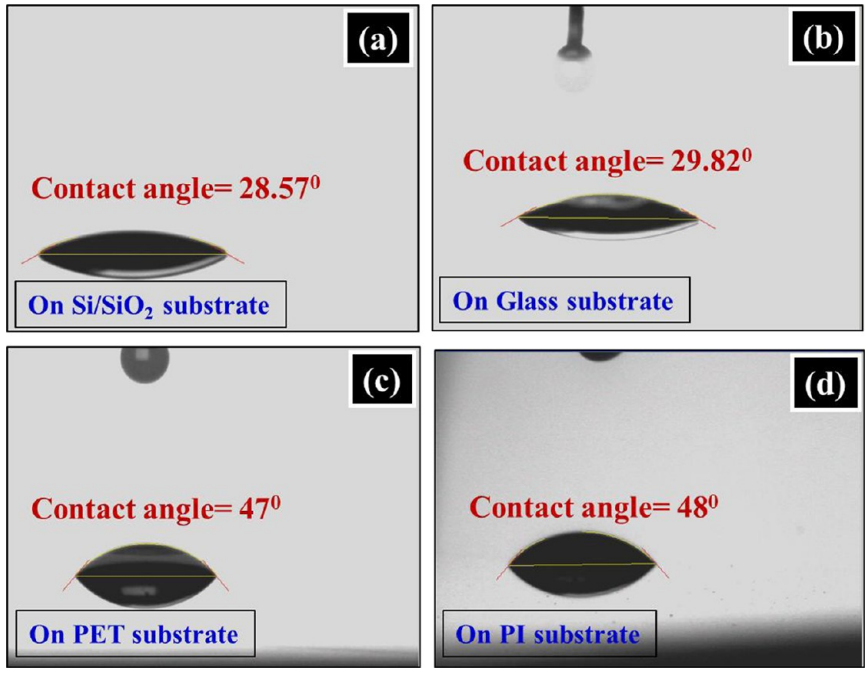

Figure 7. Contact angles of single droplets on (a) Si/SiO_2, (b) glass, (c) PET, and (d) PI substrates.

dx.doi.org/10.1021/am300689d | ACS Appl. Mater. Interfaces 2012, 4, 3300−3307

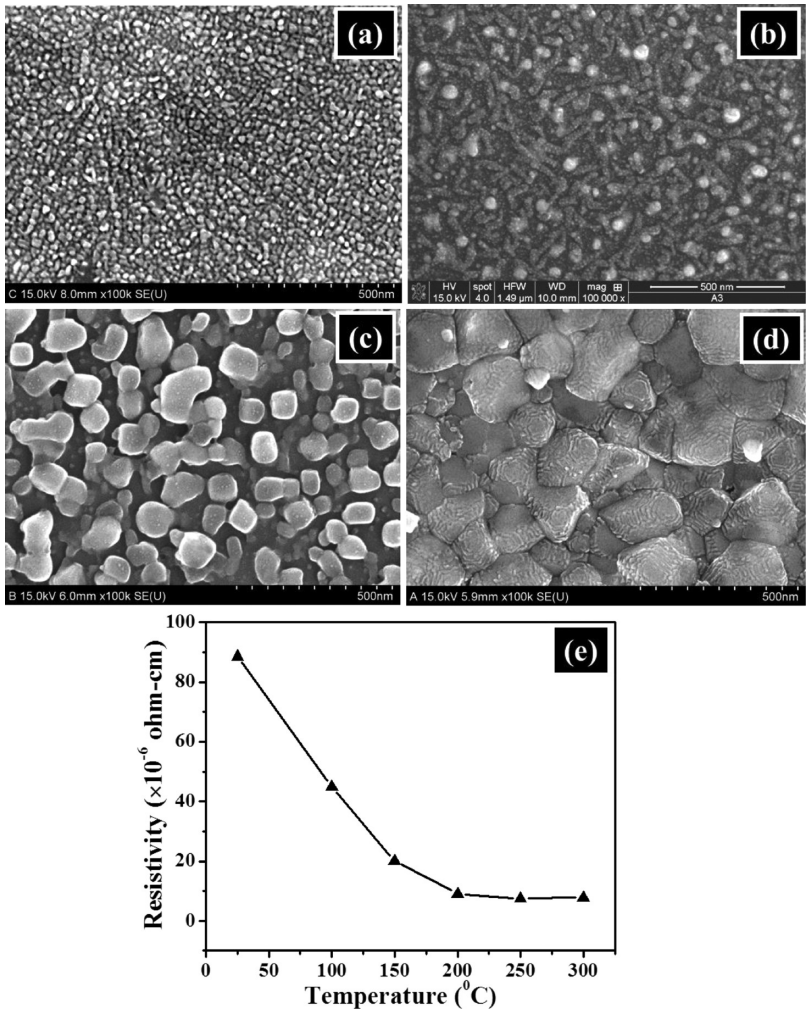

Figure 8. FESEM images for structural variation of the Ag nanoparticle films as a function of annealing temperature: (a) as-printed and annealed at (b) 100, (C) 150, and (d) 200 °C. (e) Resistivity variation of the Ag conductive lines composed of as a function of annealing temperature.

■ ASSOCIATED CONTENT

Supporting Information

FESEM and TEM images and histogram of Ag NPs synthesized at different temperatures, dynamic light scattering measurement for PVP stabilized Ag ink, CCD camera images of inkjet-printed Ag lines. This material is available free of charge via the Internet at http://pubs.acs.org.

■ AUTHOR INFORMATION

Corresponding Author

*E-mail: ybhahn@chonbuk.ac.kr. Tel: +82-(63)-270-2439. Fax: +82-(63)-270-2306.

Notes

The authors declare no competing financial interest.

■ ACKNOWLEDGMENTS

This work was supported in part by National Leading Research Laboratory program (2011-0028899) and by the World Class University program (R31-20029) funded from Korean government (MEST). The authors also thank Mr. Kwon-Jae Taek at Korea Printed Electronics Center, KBSI Jeonju branch, and Mr. Jong-Gyun Kang at CURF for taking quality contact angle measurement and SEM and TEM images, respectively.

■ REFERENCES

(1) Magdassi, S.; Grouchko, M.; Berezin, O.; Kamyshny, A. *ACS Nano* **2010**, *4*, 1943−1948.
(2) Stringer, J.; Derby, B. *Langmuir* **2010**, *26*, 10365−10372.
(3) Woo, K.; Kim, Y.; Lee, B.; Kim, J.; Moon, J. *ACS Appl. Mater. Interfaces* **2011**, *3*, 377−2382.
(4) Zhang, R.; Lin, W.; Moon, K.; Wong, C. P. *ACS Appl. Mater. Interfaces* **2010**, *2*, 2637−2645.
(5) Wu, J.-T.; Hu, S. L.-C.; Tsai, M.-H.; Hwang, W.-S. *J. Phys. Chem. C* **2010**, *114*, 4659−4662.
(6) Jang, D.; Kim, D.; Moon, J. *Langmuir* **2009**, *25*, 2629−2635.
(7) Vaseem, M.; Lee, K.-M.; Shin, J.-K.; Hahn, Y.-B. *J. Nanosci. Nanotechnol.* **2012**, *12*, 2380−2386.
(8) Zhang, Z.; Zhang, X.; Xin, Z.; Deng, M.; Wen, Y.; Song, Y. *Nanotechnology* **2011**, *22*, 425601.
(9) Lee, H. N.; Lee, Y. G.; Ko, I. H.; Hwang, E. C.; Kang, S. K. *Curr. Appl. Phys.* **2008**, *8*, 626−630.
(10) Barret, M.; Sanaur, S.; Collot, P. *Org. Electron.* **2008**, *9*, 1093−1100.
(11) Hosono, H. *Thin Solid Films* **2007**, *515*, 6000−6014.
(12) Schilinsky, P.; Waldauf, C.; Brabec, C. J. *Adv. Funct. Mater.* **2006**, *16*, 1669−1672.
(13) Koo, H. S.; Chen, M.; Pan, P. C.; Chou, L. T.; Wu, F. M.; Chang, S. J.; Kawai, T. *Displays* **2006**, *27*, 124−129.
(14) Marin, V.; Holder, E.; Wienk, M. M.; Tekin, E.; Kozodaev, D.; Schubert, U. *Macromol. Rapid Commun.* **2005**, *26*, 319−324.

(15) Gans, B. J. D.; Duineveld, P. C.; Schubert, U. S. *Adv. Mater.* **2004**, *16*, 203−213.
(16) Kim, D.; Jeong, S.; Park, B. K.; Moon, J. *Appl. Phys. Lett.* **2006**, *89*, 264101−264103.
(17) Doggart, J.; Wu, Y.; Liu, P.; Zhu, S. *ACS Appl. Mater. Interfaces* **2010**, *2*, 2189−2192.
(18) Kim, D.; Moon, J. *Electrochem. Solid-State Lett.* **2005**, *8*, J30−J33.
(19) Van Osch, T. H. J.; Perelaer, J.; de Laat, A. W. M.; Schubert, U. S. *Adv. Mater.* **2008**, *20*, 343−345.
(20) Polavarapu, L.; Manga, K. K.; Cao, H. D.; Loh, K. P.; Xu, Q.-H. *Chem. Mater.* **2011**, *23*, 3273−3276.
(21) Polavarapu, L.; Manga, K. K.; Yu, K.; Ang, P. K.; Cao, H. D.; Balapanuru, J.; Loh, K. P.; Xu, Q.-H. *Nanoscale* **2011**, *3*, 2268−2274.
(22) Shankar, R.; Groven, L.; Amert, A.; Whites, K. W.; Kellar, J. J. *J. Mater. Chem.* **2011**, *21*, 10871−10877.
(23) Volkman, S. K.; Pei, Y.; Redinger, D.; Yin, S.; Subramanian, V. *Mater. Res. Soc. Symp. Proc.* **2004**, *814*, 17.8.1−17.8.6.
(24) Jahn, S. F.; Blaudeck, T.; Baumann, R. R. *Chem. Mater.* **2010**, *22*, 3067−3071.
(25) Wang, X.; Zhuang, J.; Peng, Q.; Li, Y. D. *Nature* **2005**, *437*, 121−124.
(26) Chen, Y. Y.; Wang., X. K. *Mater. Lett.* **2008**, *62*, 2215−2218.
(27) Borodko, Y.; Habas, S. E.; Koebel, M.; Yang, P.; Frei, H.; Somorjai, G. A. *J. Phys. Chem. B* **2006**, *110*, 23052−23068.
(28) Liu, L.; Wei, T.; Guan, X.; Zi, X.; He, H.; Dai, H. *J. Phys. Chem. C* **2009**, *113*, 8595−8600.
(29) You, T.; Xu, S.; Sun, S.; Song, X. *Mater. Lett.* **2009**, *63*, 920−922.
(30) Thomas, J.; Kumar, K. P.; Mathew, S. *Sci. Adv. Mater.* **2011**, *3*, 59−65.
(31) Hofmeister, H.; Tan, G. L.; Dubiel, M. *J. Mater. Res.* **2005**, *20*, 1551−1562.
(32) Malekzadeh, M.; Halali, M. *Chem. Eng. J.* **2011**, *168*, 441−445.
(33) Mehta, S. K.; Chaudhary, S.; Kumar, S.; Gradzielski, M. *Sci. Adv. Mater.* **2011**, *3*, 196−209.
(34) Vaseem, M.; Umar, A.; Kim, S. H.; Hahn, Y.-B. *J. Phys. Chem. C* **2008**, *112*, 5729−5735.
(35) Vaseem, M.; Lee, K. M.; Kim, D. Y.; Hahn, Y.-B. *Mater. Chem. Phys.* **2011**, *125*, 334−341.
(36) Huang, N. M.; Radiman, S.; Lim, H. N.; Khiew, P. S.; Chiu, W. S.; Lee, K. H.; Syahida, A.; Hashim, R.; Chia, C. H. *Chem. Eng. J.* **2009**, *155*, 499−507.
(37) Ghaedia, M.; Sadeghian, B.; Amiri Pebdani, A.; Sahraei, R.; Daneshfar, A.; Duran, C. *Chem. Eng. J.* **2012**, *187*, 133−141.
(38) Zhao, T.; Sun, R.; Yu, S.; Zhang, Z.; Zhou, L.; Huang, H.; Du, R. *Colloids Surf., A* **2010**, *366*, 197−202.
(39) Wang, S.; Xin, H. *J. Phys. Chem. B* **2000**, *104*, 5681−5685.
(40) Witten, T. A., Jr; Sander, L. M. *Phys. Rev. Lett.* **1981**, *47*, 1400−1403.
(41) Mandal, S. K.; Hangopadhyay, A.; Chaudhuri, S.; Pal, A. K. *Vacuum* **1999**, *52*, 485−490.